



Article

High Gravity-Enhanced Direct Air Capture: A Leap Forward in CO₂ Adsorption Technology

Shufei Wang, Youzhi Liu *, Chengqian Zhang, Shuwei Guo and Yuliang Li

Shanxi Province Key Laboratory of Chemical Process Intensification, North University of China, Taiyuan 030051, China; s202104023@st.nuc.edu.cn (S.W.); b20210405@st.nuc.edu.cn (C.Z.); sz202104027@st.nuc.edu.cn (S.G.); sz202104021@st.nuc.edu.cn (Y.L.)

* Correspondence: liuyz@nuc.edu.cn

Abstract: Given the global pressure of climate change and ecological equilibrium, there is an urgent need to develop effective carbon dioxide (CO₂) capture technology. Due to its comprehensiveness and flexibility, Direct Air Capture (DAC) technology has emerged as a vital supplement to traditional emission reduction methods. This study aims to innovate Direct Air Capture (DAC) technology by utilizing the ultrasonic impregnation method to load Tetraethylpentamine (TEPA) onto alumina (Al₂O₃) as the adsorbent. Furthermore, high gravity adsorption technology is integrated to significantly enhance the efficiency of DAC. Characterization tests, including BET, FTIR, TG, XRD, and SEM-EDS, confirm the structural stability and high capture capacity of the adsorbent. Additionally, this study demonstrates the rapid and efficient capture of CO₂ from the air using TEPA-Al₂O₃ adsorbent under high gravity conditions for the first time. Under optimal conditions with TEPA loading at 15.06%, a high gravity factor of 2.67, and a gas flow rate of 30 L/min, TEPA-Al₂O₃ achieves a CO₂ adsorption capacity of 48.5 mg/g in RAB, which is an improvement of 15.56 mg/g compared to traditional fixed-bed technology. Moreover, it reaches adsorption saturation faster under high gravity conditions, exhibiting a significantly higher adsorption rate compared to traditional fixed-bed systems. Furthermore, the adsorption process better conforms to the Avrami model. Steam stripping regeneration is utilized to regenerate the adsorbent, demonstrating excellent regeneration performance and stable adsorption capacity, thereby proving its feasibility and economic benefits as a DAC technology.



Citation: Wang, S.; Liu, Y.; Zhang, C.; Guo, S.; Li, Y. High Gravity-Enhanced Direct Air Capture: A Leap Forward in CO₂ Adsorption Technology. *Atmosphere* **2024**, *15*, 238. <https://doi.org/10.3390/atmos15020238>

Academic Editor: Kumar Vikrant

Received: 31 January 2024

Revised: 14 February 2024

Accepted: 16 February 2024

Published: 18 February 2024



Copyright: © 2024 by the authors. Licensee MDPI, Basel, Switzerland. This article is an open access article distributed under the terms and conditions of the Creative Commons Attribution (CC BY) license (<https://creativecommons.org/licenses/by/4.0/>).

1. Introduction

Addressing the escalating severity of global warming and ecological imbalance, the drastic reduction of CO₂ emissions has become a critical worldwide imperative [1]. Although traditional greenhouse gas mitigation methods have shown some effectiveness, they are typically limited to specific emission points and are less effective in addressing widely dispersed emission sources and the CO₂ historically accumulated in the atmosphere [2]. Direct Air Capture (DAC) technology emerges as a versatile negative emissions technology [3] that can augment these methods, offering a more holistic and adaptable approach to the problem [4–6].

Within the global strategy to combat climate change, Direct Air Capture (DAC) technology stands out as particularly important and offers a unique pathway to achieve carbon neutrality. DAC technology operates independently of the CO₂ emission sources, allowing it to be deployed anywhere in the world without being constrained by geographical location or emission intensity [7]. Additionally, DAC technology can capture CO₂ emissions that are challenging to mitigate through other methods, such as those from the transportation and agriculture sectors. Therefore, DAC technology is an essential component of achieving long-term global climate goals.

Adsorption technology is used in different energy systems [8,9], with high selectivity for CO₂, and can be operated at room temperature and pressure, which has significant advantages over other technologies such as liquid solvent absorption or membrane separation in terms of feasibility and energy efficiency of technical implementation.

However, despite the promising prospects of DAC technology, its commercial viability is hindered by the low mass transfer efficiency resulting from capturing extremely low concentrations of CO₂ in the atmosphere (400 ppm) [10]. This difficulty in capturing DAC technology due to low mass transfer efficiency underscores the significance of selecting appropriate carbon dioxide capture materials and capture equipment. High gravity technology, an innovative process intensification technique, employs centrifugal forces from rotation to simulate a high gravity environment and boost mass transfer. Widely applied in fields such as absorption [11], distillation [12], liquid–liquid extraction and reaction [13], dust removal [14], nanomaterial fabrication [15], and adsorption [16,17]. High gravity adsorption, utilizing a rotating packed bed for an expanded gas–solid interface and rapid renewal, represents an advancement in this field. In order to further improve the efficiency of DAC technology, this study innovatively adopts the combination of high gravity adsorption technology. This study has adopted high gravity adsorption to enhance DAC's efficiency, where the increased rotational speeds in a high gravity adsorption bed markedly improve the adsorbent's interaction with CO₂ [16,18,19].

The selection of appropriate adsorbents is crucial for advancing DAC technology [10,20]. Optimal adsorbents exhibit high selectivity and adsorption capacity, robust regenerative capabilities, and cost-effectiveness. Amine-functionalized adsorption technologies are notable for their low energy and equipment costs, as well as their high selectivity [4,21–23]. Tetraethylenepentamine (TEPA), with its amine-dense structure, has demonstrated superior ultra-dilute CO₂ absorption rates [24–26]. Notably, Salestan et al. observed a 63% increase in CO₂ adsorption selectivity when TEPA was grafted onto MIL-101 [27]. These findings underscore TEPA's efficacy as an amine agent, bolstering its adsorption performance based on raw materials. Consequently, this study selected TEPA as the adsorbent due to its amine-rich structure and impressive CO₂ capture capacity. TEPA's ability to capture CO₂ with low energy input and its operational stability across various temperatures and pressures make it an ideal choice. To maximize TEPA's performance, ultrasonic impregnation is used to load it onto alumina with a high specific surface area, providing a stable physical framework and ensuring thermal and mechanical stability during CO₂ capture.

As shown in Figure 1, CO₂ in the air is captured by the adsorbent, and the adsorbent, after the completion of the capture, is regenerated by water vapor, and the regenerated adsorbent is used again for CO₂ capture, and the pure CO₂ is stored.

This study comprehensively evaluates the TEPA-Al₂O₃ adsorbent within a high gravity adsorption bed through carefully designed experiments. The TEPA-Al₂O₃ adsorbent was synthesized using ultrasonic impregnation and extensively characterized by BET, FT-IR, XRD, TGA, and SEM-EDS to determine its structural characteristics and properties. It was then used in conjunction with high gravity adsorption technology to assess its CO₂ adsorption performance from the air, examining the effects of various operational parameters on TEPA-Al₂O₃'s efficacy. To deepen our understanding of the CO₂ adsorption mechanism, kinetic models were applied to systematically analyze the process within the high gravity adsorption bed. Interpreting the model parameters and the fitting results enabled an in-depth study of the physical and chemical phenomena occurring during adsorption, thus elucidating the operating principles of the high gravity adsorption bed. This study aims to provide an economically efficient DAC solution by innovatively combining adsorbents with high gravity apparatus. This work aims to introduce a novel instrument for global climate governance, assist in achieving carbon neutrality objectives, and emphasize the importance of technological innovation in climate change mitigation strategies.

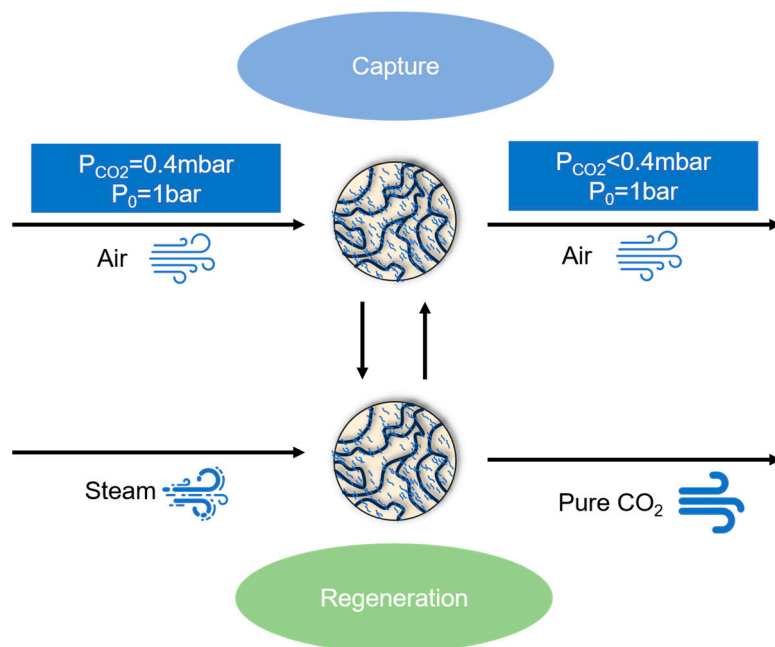


Figure 1. The cycle of amine-modified adsorbents absorbing CO₂ in air.

2. Experimental Part

2.1. Experimental Materials

Aluminum oxide (Al_2O_3) with a particle size of 2 mm was acquired from Shandong Guanghui New Materials Co., Ltd. (Shandong, China). Analytical-grade anhydrous ethanol was sourced from Tianjin Tianli Chemical Reagent Co., Ltd. (Tianjin, China). Tetraethylenepentamine (TEPA) was supplied by Shanghai Macklin Biochemical Co., Ltd. (Shanghai, China). Deionized water used for washing was obtained from an in-house purification system.

2.2. Synthesis of TEPA- Al_2O_3

Initially, the aluminum oxide was washed three times with deionized water to prepare it for subsequent use. After washing, the Al_2O_3 was dried in an oven and stored in a glass container. Secondly, TEPAethanol solutions with concentrations of 100, 150, 200, 250, and 300 mg·mL⁻¹ were prepared in beakers containing anhydrous ethanol, with thorough stirring to achieve uniform dispersion. The TEPA–ethanol solution was then transferred to another beaker in the required proportion, and an appropriate amount of the aluminum oxide carrier was added. This mixture was treated in an ultrasonicator for 4 h to allow for the uniform diffusion of TEPA molecules into the pores of the carrier. After ultrasonic treatment, the carrier impregnated with TEPA was separated from the solution by filtration and washed at least three times with anhydrous ethanol to remove any unbound TEPA. Finally, the treated sample was dried in an apparatus set at 353.15 K to remove any residual solvent. The dried sample was then stored in a glass container, ready for use.

2.3. Characterization of TEPA- Al_2O_3

The pore structure characteristics of the composite material, including its specific surface area, average pore diameter, and total pore volume, were evaluated using low-temperature nitrogen adsorption/desorption experiments conducted on a Micromeritics ASAP 2010 system (Norcross, GA, USA).

Functional groups on the surface of the composite material were identified using a NICOQ380 FTIR spectrometer (Waltham, MA, USA). FTIR spectra were recorded in the wavenumber range of 500–4000 cm⁻¹ to identify characteristic functional groups present on the material's surface.

The adsorbent's mass changes across a range of temperatures were detected using a Setaram Labsys evo thermogravimetric analyzer (Origin: Bavarian Asia, Germany, Model: STA449F3 Jupiter). During this process, the N_2 flow rate was set at $50 \text{ mL}\cdot\text{min}^{-1}$, the heating rate was $10 \text{ }^{\circ}\text{C}\cdot\text{min}^{-1}$, and the temperature testing range was set from 30 to $1000 \text{ }^{\circ}\text{C}$. The thermal stability of the alumina carrier and the TEPA–alumina composite material, as well as the proportion of polyethyleneimine in the composite material, were assessed by analyzing the TGA and DTG curves plotted.

Wide-angle X-ray diffraction (XRD) patterns ranging from 5° to 85° were obtained using a D/max-RB powder X-ray diffractometer with a Cu K α radiation source ($\lambda = 0.15406 \text{ nm}$) and a scanning speed of $8^{\circ}/\text{min}$.

Surface morphologies of carriers with different surface properties and their composite materials were analyzed using a JSM-7900F Scanning Electron Microscope (Showima City, Tokyo, Japan), yielding high-definition SEM-EDS images.

2.4. Adsorption Experiments

As shown in Figure 2, 20.0 g of previously prepared TEPA- Al_2O_3 is packed into the Rotating Adsorption Bed (RAB) to capture CO_2 from the air, with its structural parameters presented in Table 1. Air is drawn through the fan and flows through the flowmeter before entering the high gravity adsorption bed. After the adsorption process is complete, CO_2 is captured on the adsorbent, and the purified air exits the system. Throughout the entire adsorption process, a portable CO_2 detector (model: NK-500A, origin: Xi'an, China) is used to monitor the CO_2 volume concentration at the RAB outlet in real-time.

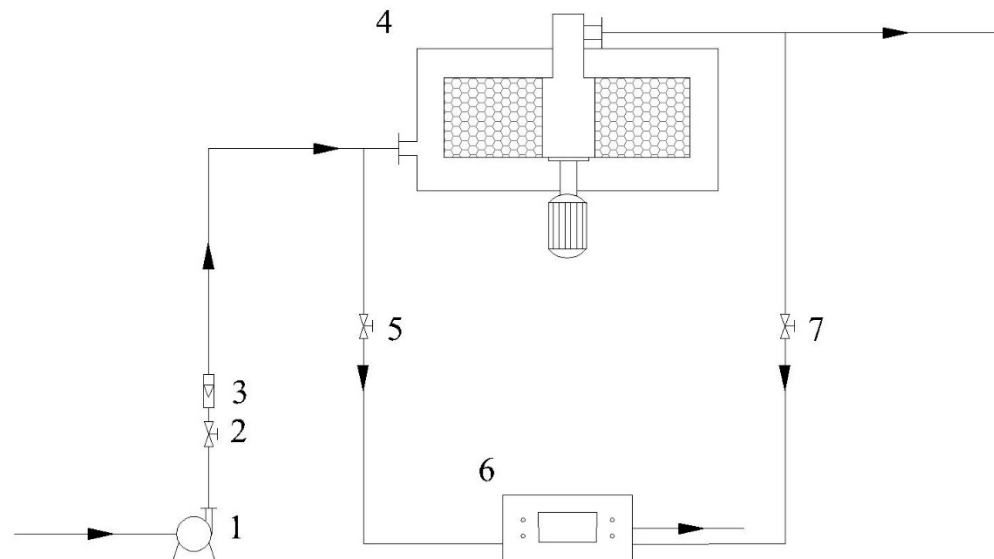


Figure 2. Schematic of the high gravity enhanced direct air CO_2 capture process using amine-modified adsorbents. 1—Fan; 2, 5, 7—Valves; 3—Flowmeter; 4—Rotating Adsorption Bed; 6—Gas Detector.

Table 1. Structural parameters of rotating packed bed.

Structure	Parameters/mm
Height (H)	54
Inner diameter (D_{in})	32
Outer diameter (D_{out})	112

The research utilizes a high gravity rotational packed bed for adsorption, where solid adsorbent particles serve as the packing material within the rotating bed, conducting the adsorption process in a high gravity environment. To compare rotational packed beds of different sizes and rotational speeds, the intensity of the high gravity field can be

represented by the dimensionless high gravity factor according to research methods in chemical engineering. The dimensionless high gravity factor (β) is defined as the ratio of the inertial acceleration (centrifugal acceleration) G to the gravitational acceleration g (9.81 m/s^2). Its expression can be simplified as follows:

$$\beta = \frac{N^2 r}{900} \quad (1)$$

where N is the rotating speed ($\text{r}\cdot\text{min}^{-1}$), and r is the radius of the rotor (m). In our study, the corresponding values of N and β are shown in Table 2.

Table 2. The relationship between rotational speed and high gravity factor in the rotating adsorption bed.

$N (\text{r}\cdot\text{min}^{-1})$	200	300	400	500	600
β	0.67	1.50	2.67	4.17	6.00

The adsorption capacity (q_t) can be calculated using Equation (2). For comparison, control experiments were also conducted in a fixed bed of the same size as the RAB, under the same reaction conditions as in the RAB experiments. All experiments were performed in triplicate, and the average values were taken to minimize measurement errors.

$$q_t = \frac{Q \cdot M_{CO_2} \cdot \int_0^t (c_t - c_0) dt}{V_m \cdot m \cdot 1000} \quad (2)$$

where q_t is the adsorption capacity ($\text{mg}\cdot\text{g}^{-1}$), Q is the gas flow rate ($\text{L}\cdot\text{min}^{-1}$), m is the mass of the adsorbent (g), c_0 and c_t are the inlet and outlet CO_2 volume concentrations (%), V_m is the molar volume of gas ($22.4 \text{ L}\cdot\text{mol}^{-1}$), and M_{CO_2} is the molar mass of CO_2 ($44 \text{ g}\cdot\text{mol}^{-1}$).

The regeneration of the adsorbent was conducted using steam stripping. The CO_2 -saturated adsorbent was dispersed in a glass container and then contacted with saturated steam at a flow rate of $1.2 \text{ g}\cdot\text{min}^{-1}$ and a temperature of 103°C for 30 min to regenerate the adsorbent. The steam stripping regeneration was repeated multiple times to evaluate the regeneration efficiency and adsorption capacity of the adsorbent.

3. Results and Discussion

3.1. Characterization of TEPA- Al_2O_3

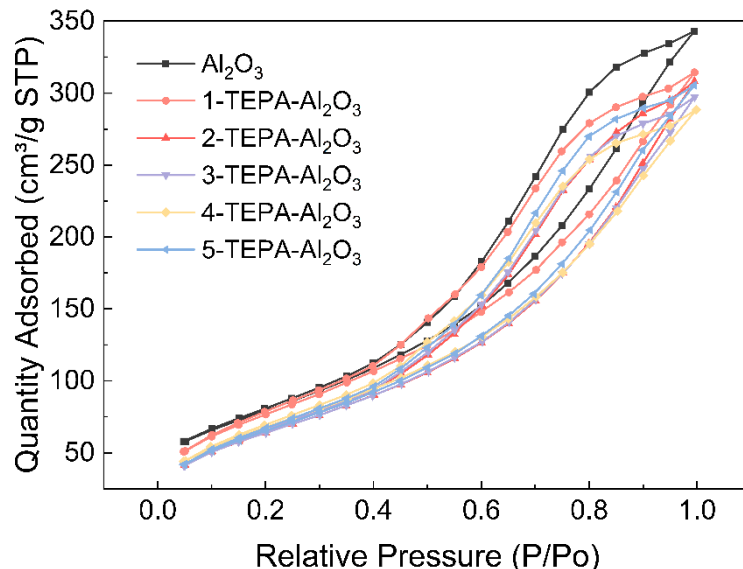
3.1.1. Analysis of Specific Surface Area, Pore Volume and Pore Size

The porosity characteristics of both Al_2O_3 and its TEPA-impregnated counterparts were thoroughly examined using N_2 adsorption–desorption measurements. Table 3 shows Pore structural properties of Al_2O_3 and TEPA- Al_2O_3 . Notably, both materials exhibited Type IV adsorption isotherms [28] accompanied by distinctive H3 hysteresis loops (Figure 3), indicative of their mesoporous nature. As the relative pressure increased, the adsorption capacities of the materials showed incremental growth until reaching saturation, while desorption occurred at a gradual pace, highlighting stable adsorption properties and the presence of specific pore sizes and structures within the porous materials. The appearance of the hysteresis loop at a relative pressure (P/P_0) around 0.40 suggested the existence of smaller mesopores within the materials. Upon impregnation with TEPA, noticeable alterations in surface area were observed. Initially, at lower TEPA concentrations, there was a slight increase in surface area, likely due to TEPA occupying smaller voids or surface defects, thereby enhancing the effective surface area of the material. However, as the concentration of TEPA increased, a plateau or minor decline in surface area was observed. This phenomenon can be attributed to the aggregation of TEPA molecules at higher concentrations, which tend to accumulate on the surface, thereby masking active sites and potentially leading to the occlusion or narrowing of minute pores. As a result, there might be a reduction in pore volume or a slight constriction of pore diameters.

Table 3. Pore structural properties of Al_2O_3 and TEPA- Al_2O_3 .

Materials	S_{BET} (m^2/g) ^a	V_{pore} (cm^3/g) ^b	d (nm) ^c	Amine Loading (%) ^d
Al_2O_3	291.10	0.49	7.29	—
1-TEPA- Al_2O_3	290.53	0.49	6.69	12.86
2-PEI- Al_2O_3	248.901	0.48	6.75	12.06
3-PEI- Al_2O_3	244.95	0.46	7.51	15.06
4-PEI- Al_2O_3	258.86	0.45	6.89	15.98
5-PEI- Al_2O_3	251.25	0.47	7.52	18.49

^a BET surface area; ^b Total pore volume; ^c Average pore size; ^d The actual value from TGA.

**Figure 3.** Nitrogen adsorption/desorption isotherms of Al_2O_3 and TEPA- Al_2O_3 .

3.1.2. Fourier Transform Infrared Spectroscopy (FT-IR)

Figure 4 displays the infrared absorption spectra obtained for both Al_2O_3 and TEPA- Al_2O_3 samples. In the IR spectrum of TEPA-modified alumina, several distinct absorption peaks are clearly evident. The peak observed at 1065 cm^{-1} is tentatively attributed to the vibrations of hydroxyl groups associated with the alumina surface, indicating Al-OH vibrational modes. Similarly, the absorption peak at 1110 cm^{-1} is typically associated with C-N stretching vibrations, likely originating from the presence of amine groups in the TEPA molecule [26]. Another notable absorption peak at 1315 cm^{-1} is likely due to the bending vibrations of the C-H bonds [29]. Moreover, the peak observed at 1569 cm^{-1} may be ascribed to either the bending vibrations of N-H or the stretching vibrations of amides and carboxylic acids [29]. Moreover, the peak observed at 1569 cm^{-1} may be ascribed to either the bending vibrations of N-H or the stretching vibrations of amides and carboxylic acids [30]. Furthermore, the peak observed at 3777 cm^{-1} possibly corresponds to the vibrations of the amine groups (N-H) [29], indicating the presence of amine functionalities in the TEPA structure. The identification and assignment of these absorption peaks suggest an interaction between TEPA and the alumina surface, potentially accompanied by chemical transformations during the modification procedure.

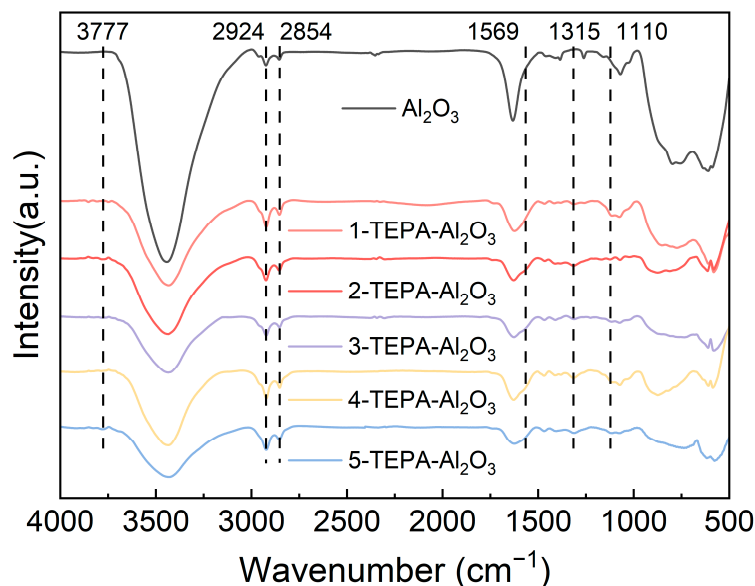


Figure 4. Infrared spectra of Al_2O_3 and TEPA- Al_2O_3 .

3.1.3. X-ray Diffraction Analysis (XRD)

As depicted in Figure 5, the XRD patterns for Al_2O_3 and TEPA- Al_2O_3 are shown. The diffraction peaks for both samples are primarily observed at 2θ values of 19.46° , 28.24° , 31.93° , 37.61° , 45.83° , 60.86° , and 67.26° . The positions of these peaks are consistent with the characteristic peaks of γ - Al_2O_3 (JCPDS No. 10-0425, JCPDS No. 34-0493), indicating that the alumina retains its Al_2O_3 crystalline structure post-TEPA loading. A comparison of the XRD patterns before and after impregnation reveals identical characteristic peak positions, suggesting that the crystal structure has not undergone fundamental changes. Additionally, the presence of distinct spike-like peaks in the XRD diffractogram may be attributed to the polycrystalline nature of the alumina microspheres used in the study [31].

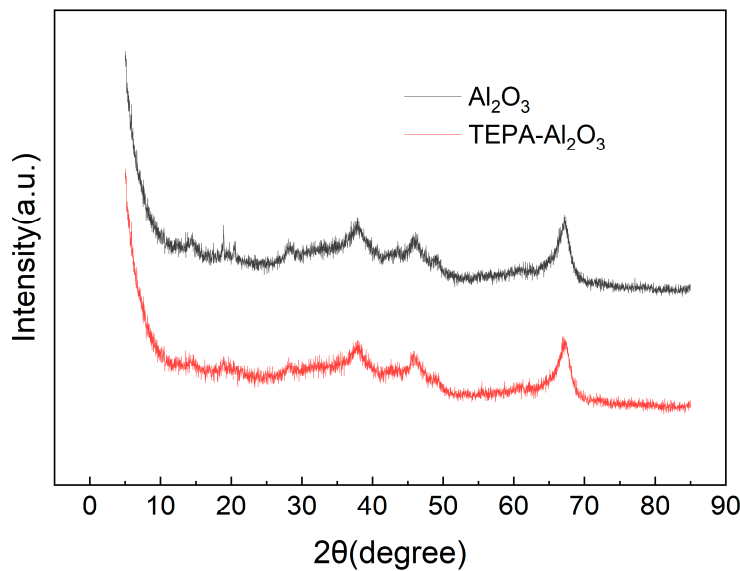


Figure 5. The curve of XRD of Al_2O_3 and TEPA- Al_2O_3 .

3.1.4. Thermal Gravimetric Analysis (TGA)

As depicted in Figure 6, the thermal behavior of both Al_2O_3 and TEPA- Al_2O_3 across a specified temperature range is illustrated. Notably, the TEPA-loaded alumina begins to exhibit weight loss at approximately 100°C . However, the thermal stability of the novel

adsorbents, prepared with varying concentrations of impregnation solution, does not show significant differences. Within the temperature range of 30 °C to 1000 °C, Al_2O_3 demonstrates only a minimal loss in mass. All adsorbents display a noticeable and consistent weight loss from 0 to 100 °C, primarily attributed to the desorption of water adsorbed on the surface and the minor decomposition of TEPA. Upon closer examination, it is observed that the weight loss for TEPA- Al_2O_3 increases above 100 °C, indicating the onset of TEPA decomposition. As the temperature rises further, the decomposition of TEPA accelerates, leading to an increased mass loss. This thermal weight loss within the specified temperature range can be utilized to calculate the loading amount of TEPA on the adsorbent. Based on these calculations, the loading amounts for 1-TEPA- Al_2O_3 , 2-TEPA- Al_2O_3 , 3-TEPA- Al_2O_3 , 4-TEPA- Al_2O_3 , and 5-TEPA- Al_2O_3 are found to be 12.86%, 12.06%, 15.06%, 15.98%, and 18.49%, respectively. The primary decomposition temperature for TEPA, which is above 100 °C, suggests that the adsorbents possess commendable thermal stability.

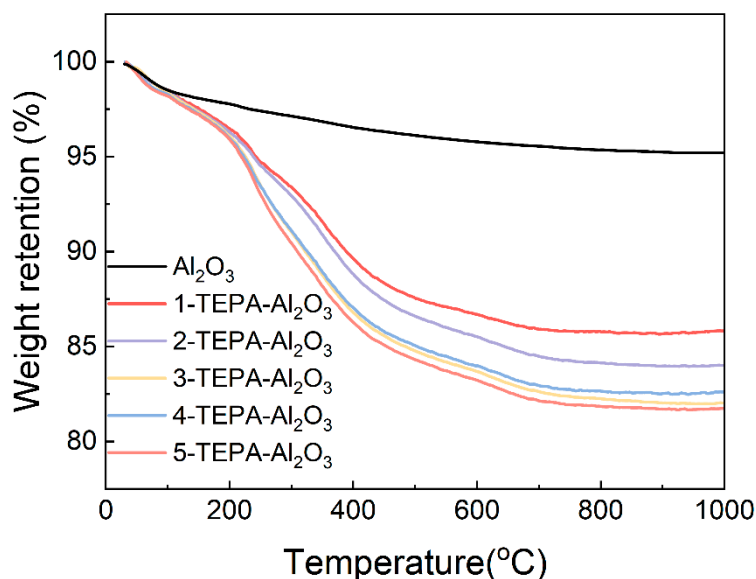


Figure 6. The curve of TG and DTG of Al_2O_3 and TEPA- Al_2O_3 in the temperature range of 30~1000 °C.

3.1.5. Scanning Electron Microscope and Energy Dispersive Spectrometer Analysis (SEM-EDS)

SEM-EDS characterization was conducted on Al_2O_3 before and after amine loading to examine the surface morphology and elemental distribution, as depicted in Figure 7. Panels (a) and (b) showcase the SEM images of Al_2O_3 and TEPA- Al_2O_3 , respectively, revealing that the alumina possesses a layered structure with abundant folds [31], providing ample space for the insertion of TEPA. The surface of TEPA- Al_2O_3 is covered with a multitude of uniformly distributed fine particles, indicating an even loading of TEPA onto the alumina surface. Energy-dispersive X-ray spectroscopy (EDS) spectra for both Al_2O_3 and TEPA- Al_2O_3 are displayed in panels (c) and (e), respectively. These spectra clearly demonstrate an enriched and homogenized distribution of nitrogen (N) in the adsorbent subsequent to TEPA loading. Panel (d) illustrates the elemental distribution for Al_2O_3 , and upon approximate estimation, the relative percentage contents for C, O, and Al elements are approximately 43.02%, 39.01%, and 17.97%, respectively. Following the loading of TEPA onto the adsorbent, in addition to C, O, and Al, the presence of the N element is also detected, with an estimated relative percentage content of approximately 7.35%. These results collectively indicate that TEPA has been uniformly loaded onto the surface of Al_2O_3 .

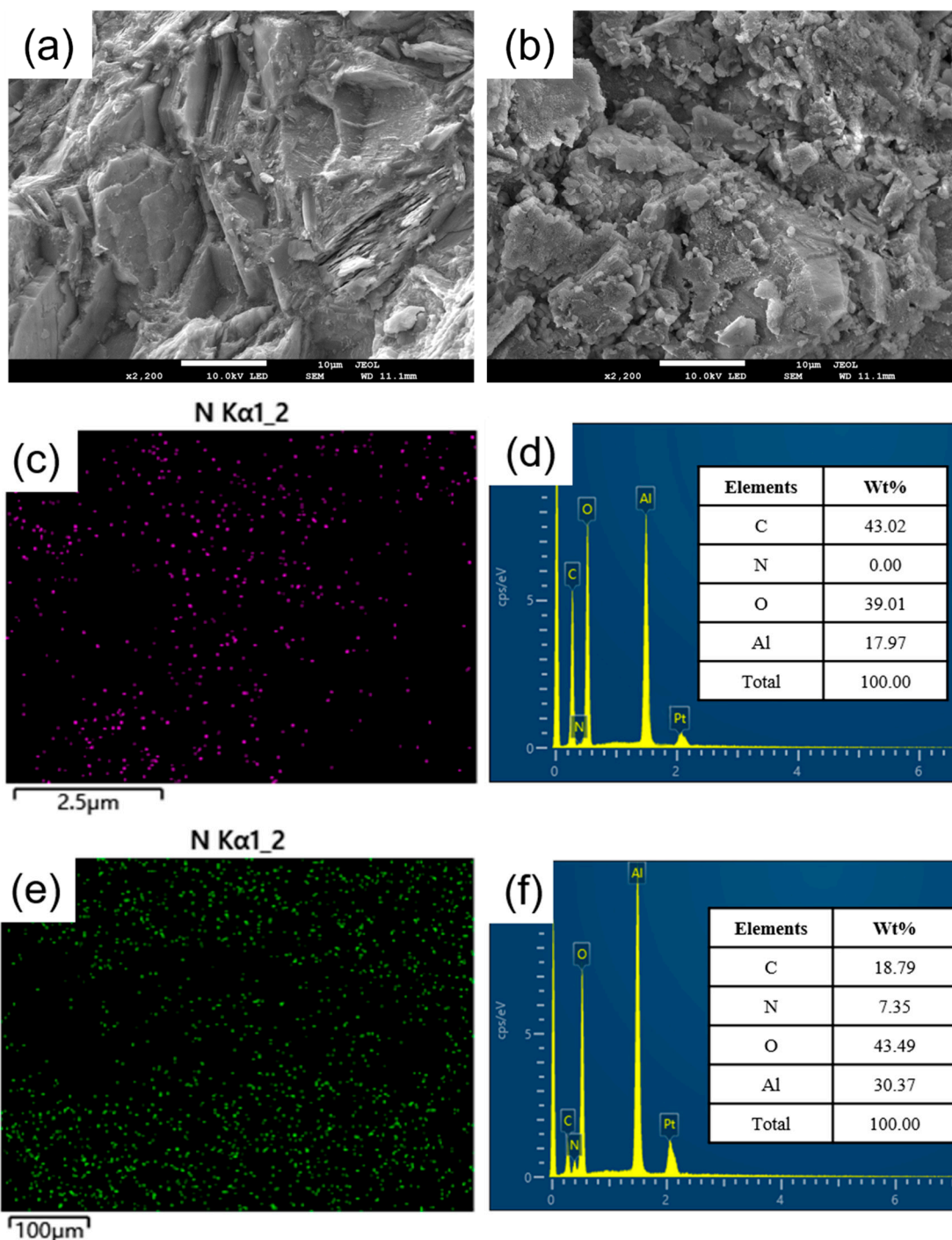


Figure 7. (a) Scanning Electron Microscope (SEM) micrograph of Al_2O_3 ; (b) SEM micrograph of TEPA- Al_2O_3 ; (c) Energy-Dispersive X-ray Spectroscopy (EDS) spectrum for nitrogen (N) on Al_2O_3 ; (d) Elemental mapping for Al_2O_3 ; (e) EDS spectrum for nitrogen (N) on TEPA- Al_2O_3 ; (f) Elemental mapping for TEPA- Al_2O_3 .

3.2. Impact of Rotating Adsorption Bed (RAB) Operational Parameters on the Adsorption Performance of TEPA- Al_2O_3

Using the quantity of CO_2 adsorption as the evaluation metric, this study explores the impact of different TEPA loading amounts, varying factors of high gravity, as well as distinct inlet gas flow rates on the CO_2 adsorption performance of TEPA- Al_2O_3 from air.

3.2.1. The Effect of TEPA Loading on CO₂ Capture from Air

At 25 °C, by keeping the inlet gas flow rate constant at 30 L/min and the high gravity factor at 1.5, the impact of varying TEPA concentrations on the absorption of CO₂ from the air by amine-modified adsorbents was investigated, with results illustrated in the accompanying Figure 8. The results indicate a significant variation in CO₂ adsorption capacity in response to changes in TEPA loading. The Al₂O₃ without TEPA loading exhibited an adsorption capacity of only 2.2 mg/g. As the TEPA concentration increased, the adsorption capacity also gradually improved, with 4-TEPA-Al₂O₃ reaching a maximum value of 48.5 mg/g. This enhancement is attributed to the increased number of active sites available for interaction due to higher TEPA loadings, which increases the adsorbent surface affinity for CO₂. Furthermore, the experiments revealed that the time to reach adsorption saturation varied with TEPA concentration. Within a certain range, the time required to achieve adsorption saturation first increased and then decreased with rising TEPA loadings. This trend may reflect variations in adsorption rates at different TEPA loadings, suggesting an optimal CO₂ adsorption rate at specific TEPA concentrations. Notably, among the various TEPA-Al₂O₃ adsorbents studied, 4-TEPA-Al₂O₃ demonstrated the highest CO₂ adsorption capacity (reaching 48.5 mg/g) and was thus selected for subsequent experimentation.

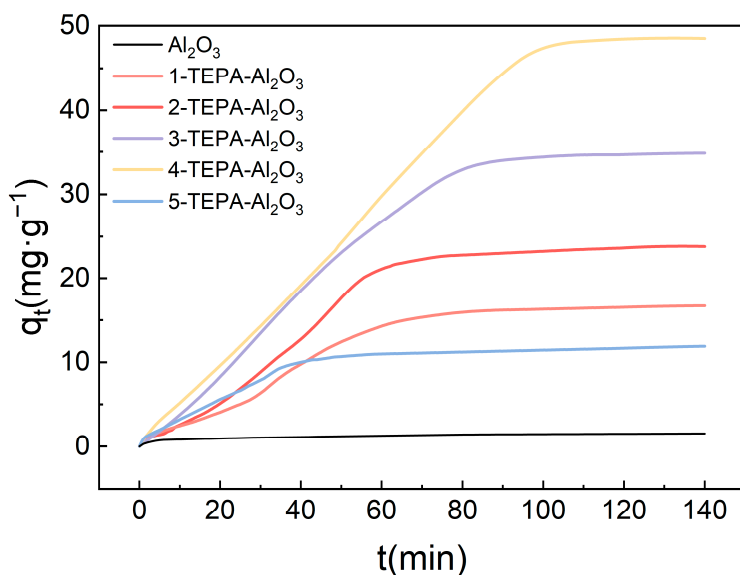


Figure 8. The influence of TEPA impregnation solution concentration on the CO₂ adsorption performance of amine-modified adsorbents.

3.2.2. The Impact of the High gravity Factor on CO₂ Capture from Air

Figure 9 illustrates the influence of the high gravity factor on the CO₂ adsorption performance of amine-modified adsorbents. It is evident that as the high gravity factor gradually increases, there is a corresponding enhancement in the adsorption capacity. Initially, the adsorption capacity shows an upward trend with the increasing high gravity factor. This is attributed to the fact that a higher gravity factor promotes more frequent collisions between gas molecules and the adsorbent surface, thus accelerating the adsorption rate. Within the range of experimental parameters, an increase in adsorption capacity is observed, although the rate of increase remains moderate. As the high gravity factor is further elevated, it continues to augment the collision rate between gas molecules and the adsorbent surface. This enhancement in collision frequency further accelerates the adsorption rate, consequently shortening the time required to reach adsorption saturation. The findings highlight the significant role of the high gravity factor in influencing the kinetics of CO₂ adsorption. By facilitating more efficient mass transfer and enhancing

the interaction between gas molecules and the adsorbent surface, higher gravity factors contribute to improved adsorption performance.

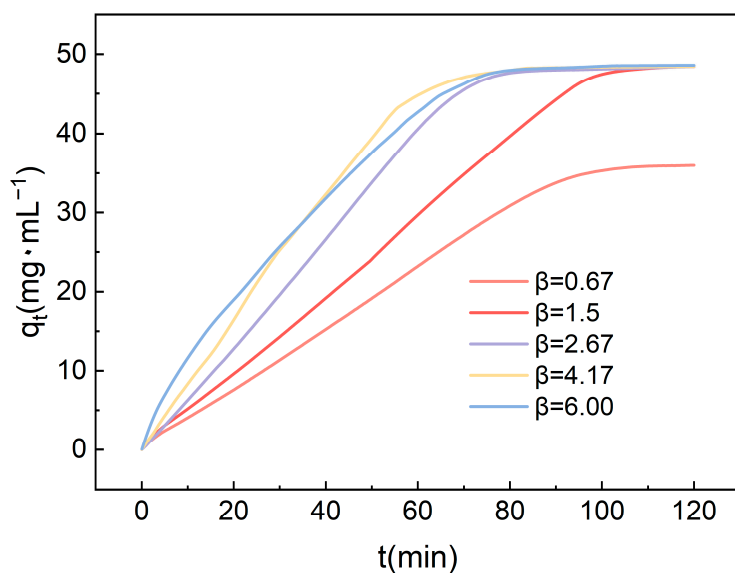


Figure 9. The impact of the high gravity factor on the CO_2 adsorption performance of amine-modified adsorbents.

Although higher high gravity factors assist in increasing the frequency of collisions, adverse flow phenomena may lead to a reduced rate of adsorption. An excessively high high gravity factor might cause uneven movement of gas molecules within the packed bed, potentially leading to channeling effects. Under such circumstances, a portion of the CO_2 may bypass the adsorbent surface and pass directly through the bed without sufficient contact, resulting in a decreased adsorption rate. From the graph, it is evident that TEPA-Al₂O₃ reaches adsorption saturation within 70 min at a high gravity factor of 4.17, which has been selected for use in subsequent studies.

3.2.3. The Effect of Inlet Air Flow Rate on the Capture of CO_2 from Air

Based on the experimental outcomes, under the condition of a high gravity factor of 4.17, the impact of varying gas flow rates on the adsorption of carbon dioxide from the air using 4-TEPA-Al₂O₃ was investigated, with the results depicted in the accompanying Figure 10. At lower flow rates (10 L/min and 15 L/min), the adsorption capacity approached saturation within 200 min but did not achieve a saturated state. Under these two flow rate conditions, the duration for the adsorbent to reach saturation was extended. However, as the gas flow rate was further increased, the adsorption capacity reached the same saturation level of $48.4 \text{ mg}\cdot\text{g}^{-1}$, and the time required to achieve saturation gradually decreased. At a flow rate of 25 L/min, adsorption saturation was attained around 80 min. This trend may suggest that the gas flow rate exerts a significant influence on the adsorption kinetics. At low flow rates, the adsorbent has ample time to interact with CO_2 , hence achieving a relatively high adsorption capacity even at reduced flow rates. Conversely, with increased gas flow rates, the residence time of the gas on the adsorbent surface diminishes, resulting in a greater volume of gas contacting the adsorbent per unit time, yet the number of available adsorption sites on the surface remains unchanged. Consequently, at higher flow rates, the rate of adsorption is quicker, and the time to reach the same level of adsorption capacity is shorter, ultimately converging to the same adsorption quantity.

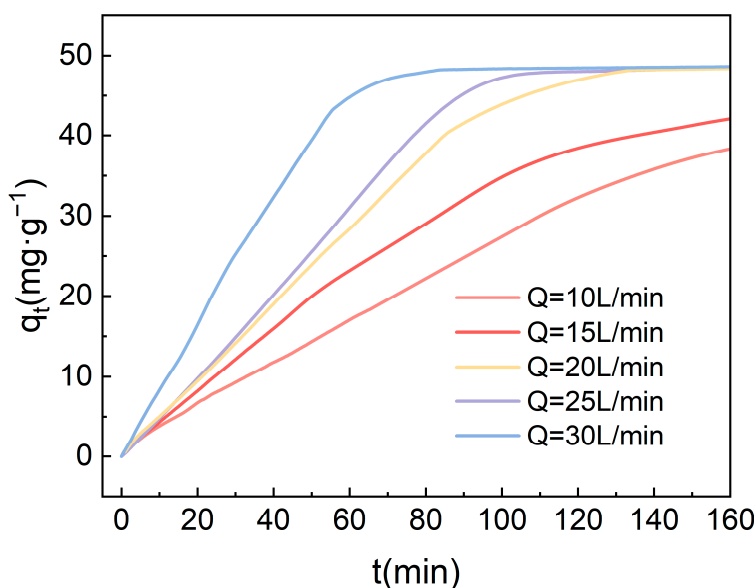


Figure 10. The impact of gas flow rate on the CO₂ adsorption performance of amine-modified adsorbents.

3.3. Kinetic Analysis of CO₂ Adsorption from Air by Amine-Modified Adsorbents

For amine-modified adsorbents tasked with capturing CO₂ from the air, the adsorption performance is influenced not only by the physicochemical properties of the adsorbent itself but also by the rate of adsorption. The adsorption rate is a critical factor affecting the efficiency of CO₂ uptake from the air by adsorbents and can provide essential engineering parameters for the practical application of these materials. Consequently, studying the adsorption kinetics and rates is key to exploring the process and mechanism of CO₂ adsorption from the air. Currently, numerous adsorption kinetic models are available to investigate the rate of gas adsorption reactions on the surface of porous solids. In this paper, three models are employed to analyze the kinetics of CO₂ adsorption onto amine-modified adsorbents: Lagergren's pseudo-first-order model, Ho's pseudo-second-order model, and the Avrami fractional-order kinetics model. These models were selected because they are more apt to describe the CO₂ adsorption process on amine-modified materials, where the adsorption rate is limited by the kinetics of surface reactions [32].

3.3.1. Lagergren's Pseudo-First-Order Adsorption Kinetics Model

The Lagergren pseudo-first-order kinetic model is commonly utilized to determine whether the adsorption reaction follows a physisorption mechanism. This model is straightforward and particularly suitable for adsorption processes where surface adsorption predominates. It postulates that at adsorption equilibrium, the interaction between the gas and the solid surface is reversible, and the adsorption rate is directly proportional to the difference between the equilibrium adsorption capacity and the quantity of adsorbate at time t. The model has been widely applied in the analysis of dynamic adsorption data and in the design of adsorption processes. Its formula is expressed as follows:

$$\frac{dq_t}{dt} = k_1(q_e - q_t) \quad (3)$$

Integrating Equation (2) yields Equation (3):

$$q_t = q_e \left(1 - e^{(-k_1 t)} \right) \quad (4)$$

where q_t is the adsorption capacity at time t (mg/g); q_e is the equilibrium adsorption capacity (mg/g); k_1 is the rate constant of the pseudo-first-order model (min^{-1}); t is the adsorption time (min).

3.3.2. Ho's Pseudo-Second-Order Adsorption Kinetics Model

The Ho pseudo-second-order kinetic model assumes that the rate of adsorption is related to the availability of active sites on the surface of the adsorbent and is primarily applicable to chemisorption mechanisms. This model can more comprehensively describe the adsorption mechanism, providing a preliminary assessment and rate characterization of the adsorption process. It is suitable for the adsorption processes of most porous adsorbents. Its expression is as follows:

$$\frac{dq_t}{dt} = k_2(q_e - q_t)^2 \quad (5)$$

Integrating Equation (4) results in Equation (5):

$$\frac{t}{q_t} = \frac{t}{q_e} + \frac{1}{k_2 q_e^2} \quad (6)$$

where q_t is the adsorption capacity at time t (mg/g); q_e is the equilibrium adsorption capacity (mg/g); k_2 is the rate constant for pseudo-second-order adsorption ($\text{g}\cdot\text{mg}^{-1}\cdot\text{min}^{-1}$); t is the adsorption time (min).

3.3.3. Avrami's Fractional-Order Kinetics Model

The pseudo-first-order and pseudo-second-order kinetic models are used to describe the physical and chemical adsorption mechanisms of adsorption reactions. Nevertheless, adsorption behavior frequently results from the combined effects of physical and chemical adsorption processes. The Avrami fractional-order kinetic model, initially developed for simulating crystallization and particle nucleation processes, is now also adopted to study the dynamic adsorption behaviors of amine-modified adsorbents [33]. This model is adept at depicting the concurrent contribution of both physical and chemical adsorption in the adsorption mechanism. Its mathematical representation is given by:

$$\frac{dq_t}{dt} = k_a^n t^{n-1} (q_e - q_t) \quad (7)$$

Upon integrating Equation (6), we obtain Equation (7):

$$q_t = q_e \left[1 - e^{-(k_a t)^n} \right] \quad (8)$$

where q_t is the adsorption capacity at time t (mg/g); q_e is the equilibrium adsorption capacity (mg/g); k_a represents the adsorption rate constant (min^{-1}); t is the adsorption time (min).

In this study, a Rotating Adsorption Bed was employed as the adsorption apparatus, utilizing amine-modified adsorbents to directly capture CO_2 from the air. Unlike conventional fixed beds, the adsorbent within the RAB is in a state of disordered rolling due to the action of centrifugal force, allowing for omnidirectional contact between the adsorbent and air rather than merely flowing upwards from the bottom of the adsorption layer. Based on this unique mode of contact, further performance evaluations revealed significant differences between the RAB and traditional fixed beds under a flow rate (Q) of 20 L/min and a dimensionless high gravity parameter (β) of 4.17, with specific results depicted in Figure 11. Table 4 shows the principal parameters for the kinetics model fitting of CO_2 adsorption from air on TEPA-Al₂O₃.

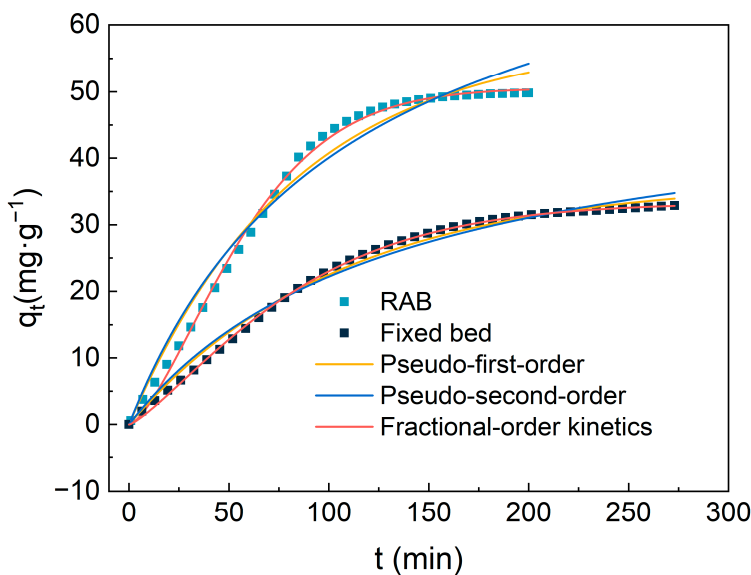


Figure 11. The comparison of kinetic model results and experimental CO_2 adsorption amounts for 4-TEPA- Al_2O_3 in the Rotating Adsorption Bed (RAB) and fixed bed.

Table 4. The principal parameters for the kinetics model fitting of CO_2 adsorption from air on TEPA- Al_2O_3 .

	The Pseudo-First-Order Model			The Pseudo-Second-Order Model			Avrami's Fractional-Order Kinetics Model			
	q_e mg/g	k_1 min^{-1}	R^2	q_e mg/g	k_2 g/(mg·min)	R^2	q_e mg/g	k_a min^{-1}	n	R^2
Fixed bed	36.65	0.009	0.992	54.69	1.4×10^{-4}	0.985	33.31	0.011	1.35	0.999
RAB	58.17	0.012	0.978	84.08	1.1×10^{-4}	0.969	50.56	0.015	1.48	0.997

The adsorption mechanism of CO_2 in air can be divided into two stages: rapid adsorption during the initial phase and a subsequent slow approach to equilibrium. In the initial phase, the abundance of active sites on the surface of the amine-modified material allows for quick adsorption of CO_2 , exhibiting a near-linear relationship with time. As these active sites become increasingly occupied, the rate of adsorption decreases due to the necessity for CO_2 to diffuse into deeper pores. Furthermore, it is evident from the graph that in the RAB, the adsorbent reaches saturation in a shorter time with a larger adsorption capacity. Compared to the traditional fixed bed method, the adsorption capacity in the RAB increased by 15.56 mg/g. The steeper slope of the adsorption curve within the RAB indicates high-*in*-or adsorption performance. To address this phenomenon, three different kinetic models were utilized for fitting and analysis.

These models demonstrated varying degrees of suitability in predicting the adsorption behavior of TEPA- Al_2O_3 for CO_2 . Among them, the pseudo-first-order and pseudo-second-order kinetic models were somewhat inaccurate in certain respects. Especially in the early stages of adsorption, the pseudo-first-order model overestimated the amount of CO_2 adsorbed, while in the stages approaching equilibrium, the predicted values of the model deviated from the actual values. In contrast, the Avrami model exhibited the best fit for the adsorption data, with the predicted adsorption capacity closely matching the experimental values and correlation coefficients (R^2) of 0.999 and 0.997 in the fixed bed and Rotating Adsorption Bed (RAB), respectively. This indicates the simultaneous occurrence of physical and chemical adsorption in the process. Furthermore, the adsorption rate constants obtained from the fitting of the three models suggest that the adsorption rate in the high centrifugal bed is significantly higher than that in the solid bed. This advantage is attributed to the continuous dynamic renewal of the adsorption medium under high

centrifugal forces, promoting a more efficient renewal of the gas–solid interface, thereby accelerating the adsorption process.

3.4. Regeneration of Amine-Modified Adsorbents

The continuous reuse of adsorbent materials is a practice in line with ecological sustainability principles, contributing to waste reduction, raw material savings, and decreased energy consumption, which aligns with the objectives of environmental protection and sustainable development strategies. Under the optimal conditions identified in previous research, we applied steam stripping technology to reactivate the amine-modified adsorbent materials and recorded the regeneration effects. Figure 12 demonstrates that after several regeneration cycles, the adsorbent still exhibited a high CO₂ capture capacity (40.32 mg·g⁻¹), with only a slight performance decay. These results highlight the superior regenerative potential and enduring stability of the adsorbent material. The steam regeneration process can periodically refresh the activity of the adsorbent material, removing the attached carbon dioxide and enabling the material's cyclic reapplication. By economically regenerating the adsorbent, we not only efficiently recover and recycle valuable adsorptive resources but also save on energy expenses. This practice of resource recycling is greatly beneficial for environmental protection and the advancement of sustainability, as well as for reducing economic costs and enhancing overall economic value.

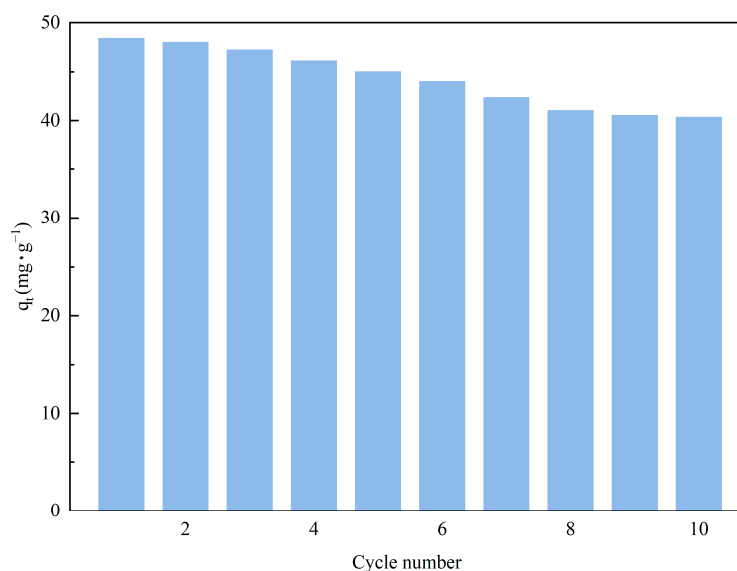


Figure 12. Cyclic adsorption performance of TEPA-Al₂O₃.

Conversely, Table 5 meticulously documents the CO₂ adsorption performance of different amine-modified adsorbents in the atmosphere. The adsorbent used in this study exhibited higher adsorption capacity compared to most other materials in the control group. This emphasizes the potential of our research in capturing atmospheric CO₂. Subsequent cyclic testing has revealed that these adsorbents maintain excellent stability, high recovery, and adsorption efficiencies over repeated use, which are crucial for sustainable operation in practical applications. Furthermore, the relatively low amine loading levels utilized in this work imply not only a more economical use of raw materials during production but also potential reductions in energy consumption and operational costs during the adsorbent regeneration process. Lower amine loading may also reduce corrosion issues and operational risks, thereby contributing to the extended lifespan of the equipment and reduced maintenance costs. This cost-benefit analysis underscores the potential economic advantages of our study for industrial applications, providing a positive outlook for future commercialization processes.

Table 5. Comparison of adsorbents of CO₂ in some literature and this work.

Support	Amine	CO ₂ (ppm)	Adsorption Capacity (mg/g)	Regeneration Temperature (°C)	Cyclic Adsorption Capacity (mg/g)	Ref.
γ-Al ₂ O ₃	PEI	400 ppmCO ₂ /Ar	45.32	105	33.88	[34]
SBA-15	PEI	400 ppmCO ₂ /Ar	14.08	105	2.64	[34]
γ-Al ₂ O ₃	20wt%PEI	400 ppm CO ₂ /Ar	25.52	60	31.24	[35]
MCF ^a	PAA ^b	400 ppm/Ar	37.84	120	36.08	[36]
MCF	PEIBr ^c	400 ppm/Ar	76.56	120	74.8	[36]
zeolite	PEI	400 ppmCO ₂	28.16	25	28.16	[37]
Zeolite Y	TEPA	0.5% CO ₂	49.28	100	47.96	[38]
silica	PEI	35.6% CO ₂	35.64	—	—	[39]
γ-Al ₂ O ₃	TEPA	400 ppm/air	48.5	105	40.32	this work

^a MCF, silica mesocellular foam; ^b PAA, Synthesis of Poly(allylamine); ^c PEIBr, branched PEI.

4. Conclusions

In this study, a novel amine-functionalized adsorbent, TEPA-Al₂O₃, with efficient CO₂ adsorption performance, was successfully prepared using the ultrasonic impregnation method. Structural and performance characterizations confirmed the uniform distribution of TEPA on the Al₂O₃ support and the excellent specific surface area, pore size, and pore volume of the formed adsorbent.

This work innovatively combined the supergravity adsorption technique to determine the optimal operating conditions for the adsorbent. Under these conditions, TEPA-Al₂O₃ exhibited a maximum saturated adsorption capacity of 48.5 mg/g and a higher adsorption rate constant compared to traditional fixed-bed systems. These findings demonstrate the advantages of the supergravity adsorption technique in improving the rate of the adsorption process. Furthermore, our adsorbent showed significant stability during repeated use and regeneration processes, maintaining an adsorption capacity of 40.32 mg/g even after 10 regeneration cycles. This result highlights not only the good durability of the adsorbent but also its potential value in practical applications, especially in achieving sustainable direct air capture technologies.

Based on this study, we anticipate future research to further develop, including exploring the applicability of the ultrasonic impregnation method to prepare other types of adsorbents, investigating CO₂ adsorption under a wider range of temperature, humidity, and other conditions in a supergravity field, optimizing the production process of TEPA-Al₂O₃ to enhance its performance, and evaluating its practicality in different industrial application scenarios. Additionally, the development of new low-energy regeneration strategies will be an important direction for further research to reduce operational costs and improve the overall sustainability of the system.

Author Contributions: Y.L. (Youzhi Liu): conceptualization, investigation, methodology, formulation or evolution of overarching research goals and aims, supervision; C.Z., S.G., and Y.L. (Yuliang Li): development or design of methodology, data curation; S.W.: conceptualization, methodology, investigation, data curation, writing—original draft, writing—review and editing. All authors have read and agreed to the published version of the manuscript.

Funding: This research was funded by “the Graduate Science and Technology Project Funding North University of China”, grant number 20221830.

Institutional Review Board Statement: Not applicable.

Informed Consent Statement: Not applicable.

Data Availability Statement: The data presented in this study are available on request from the corresponding author. The data are not publicly available due to confidentiality of test data.

Conflicts of Interest: The authors declare that they have no known competing financial interests or personal relationships that could have appeared to influence the work reported in this paper.

Nomenclature

DAC	Direct Air Capture
TEPA	Tetraethylenepentamine
Al_2O_3	Alumina
BET	Brunner–Emmet–Teller measurements
FTIR	Fourier Transform Infrared Spectroscopy
TG	Thermal Gravimetric
XRD	X-ray Diffraction
SEM-EDS	Scanning Electron Microscope and Energy Dispersive Spectrometer analysis
RAB	Rotating Adsorption Bed
H	Height, mm
D_{in}	Inner diameter, mm
D_{out}	Outer diameter, mm
N	Rotating speed, $\text{r} \cdot \text{min}^{-1}$
r	Radius of the rotor, m
β	High gravity factor
q_t	Adsorption capacity, $\text{mg} \cdot \text{g}^{-1}$
Q	Gas flow rate, $\text{L} \cdot \text{min}^{-1}$
M	Mass of the adsorbent, g
C_0 and C_t	Inlet and outlet CO_2 volume concentrations (%)
V_m	Molar volume of gas ($22.4 \text{ L} \cdot \text{mol}^{-1}$)
M_{CO_2}	Molar mass of CO_2 ($44 \text{ g} \cdot \text{mol}^{-1}$)
S_{BET}	BET surface area, m^2/g
V_{pore}	Total pore volume, cm^3/g
q_e	Equilibrium adsorption capacity, mg/g
k_1	Rate constant of the pseudo-first-order model, min^{-1}
t	Adsorption time, min
k_2	Rate constant for pseudo-second-order adsorption, $\text{g} \cdot \text{mg}^{-1} \cdot \text{min}^{-1}$
k_a	Adsorption rate constant of Avrami's Fractional-Order Kinetics Model, min^{-1}

References

- Ozkan, M.; Nayak, S.P.; Ruiz, A.D.; Jiang, W. Current status and pillars of direct air capture technologies. *iScience* **2022**, *25*, 103990. [[CrossRef](#)] [[PubMed](#)]
- Leeson, D.; Mac Dowell, N.; Shah, N.; Petit, C.; Fennell, P.S. A Techno-economic analysis and systematic review of carbon capture and storage (CCS) applied to the iron and steel, cement, oil refining and pulp and paper industries, as well as other high purity sources. *Int. J. Greenh. Gas Control* **2017**, *61*, 71–84. [[CrossRef](#)]
- Abanades, J.C.; Criado, Y.A.; White, H.I. Direct capture of carbon dioxide from the atmosphere using bricks of calcium hydroxide. *Cell Rep. Phys. Sci.* **2023**, *4*, 101339. [[CrossRef](#)]
- Jones, C.W. CO_2 Capture from dilute Gases as a Component of Modern Global Carbon Management. *Annu. Rev. Chem. Biomol. Eng.* **2011**, *2*, 31–52. [[CrossRef](#)]
- Castro-Muñoz, R.; Zamidi Ahmad, M.; Malankowska, M.; Coronas, J. A new relevant membrane application: CO_2 direct air capture (DAC). *Chem. Eng. J.* **2022**, *446*, 137047. [[CrossRef](#)]
- Lee, J.W.; Ahn, H.; Kim, S.; Kang, Y.T. Low-concentration CO_2 capture system with liquid-like adsorbent based on monoethanolamine for low energy consumption. *J. Clean. Prod.* **2023**, *390*, 136141. [[CrossRef](#)]
- Leoncio, G.; Fennell, P.S.; Shah, N. Analysis of Technologies for Carbon Dioxide Capture from the Air. *Appl. Sci.* **2022**, *12*, 8321. [[CrossRef](#)]
- Aboelmaaref, M.M.; Zhao, J.; Zayed, M.E.; Li, Y.; Gu, L.; Askalany, A.A.; Ghazy, M.; Alsaman, A.S.; Ali, E.S. Design and dynamic numerical modeling of a hybrid reverse osmosis/adsorption-based distillation system driven by solar dish Stirling engine for enhanced performance and waste heat recovery. *Process Saf. Environ. Prot.* **2023**, *180*, 324–338. [[CrossRef](#)]
- Sadek, S.; Deng, S.; Zhao, J.; Zayed, M.E. Solar-powered adsorption-based atmospheric water harvesting systems: Principles, materials, performance analysis, and configurations. *Sustain. Energy Technol. Assess.* **2022**, *54*, 102874. [[CrossRef](#)]
- Liu, R.-S.; Xu, S.; Hao, G.-P.; Lu, A.-H. Recent Advances of Porous Solids for Ultradilute CO_2 Capture. *Chem. Res. Chin. Univ.* **2022**, *38*, 18–30. [[CrossRef](#)]
- Jiao, W.; Yang, P.; Qi, G.; Liu, Y. Selective absorption of H_2S with High CO_2 concentration in mixture in a rotating packed bed. *Chem. Eng. Process. Process Intensif.* **2018**, *129*, 142–147. [[CrossRef](#)]
- Li, X.; Liu, Y.; Li, Z.; Wang, X. Continuous Distillation Experiment with Rotating Packed Bed. *Chin. J. Chem. Eng.* **2008**, *16*, 656–662. [[CrossRef](#)]

13. Jiao, W.; Liu, Y.; Qi, G. Micromixing Efficiency of Viscous Media in Novel Impinging Stream-Rotating Packed Bed Reactor. *Ind. Eng. Chem. Res.* **2012**, *51*, 7113–7118. [[CrossRef](#)]
14. Qi, G.; Cheng, S.; Liu, Y.; Guo, Q. Pilot scale test of wet dust removal by high gravity intensification technology in fertilizer plant. *J. Environ. Chem. Eng.* **2021**, *9*, 106424. [[CrossRef](#)]
15. Fan, H.-L.; Zhou, S.-F.; Gao, J.; Liu, Y.-Z. Continuous preparation of Fe_3O_4 nanoparticles through Impinging Stream-Rotating Packed Bed reactor and their electrochemistry detection toward heavy metal ions. *J. Alloys Compd. Interdiscip. J. Mater. Sci. Solid-State Chem. Phys.* **2016**, *671*, 354–359. [[CrossRef](#)]
16. Guo, Q.; Liu, Y.; Qi, G.; Jiao, W. Study of low temperature combustion performance for composite metal catalysts prepared via rotating packed bed. *Energy* **2019**, *179*, 431–441. [[CrossRef](#)]
17. Ren, H.; Li, H.; Shen, H.; Liu, Y. Experimental study on CO_2 adsorption with silica-supported ionic liquid in a high gravity reactor. *Fuel* **2023**, *331*, 125932. [[CrossRef](#)]
18. Guo, Q.; Liu, Y.; Qi, G.; Jiao, W. Adsorption and desorption behaviour of toluene on activated carbon in a high gravity rotating bed. *Chem. Eng. Des.* **2019**, *143*, 47–55. [[CrossRef](#)]
19. Guo, Q.; Liu, Y.; Qi, G. Application of high-gravity technology NaOH-modified activated carbon in rotating packed bed (RPB) to adsorb toluene. *J. Nanopart. Res.* **2019**, *21*, 175. [[CrossRef](#)]
20. Dutcher, B.; Fan, M.; Russell, A.G. Amine-based CO_2 capture technology development from the beginning of 2013—A review. *ACS Appl. Mater. Interfaces* **2015**, *7*, 2137–2148. [[CrossRef](#)] [[PubMed](#)]
21. Ferella, F.; Puca, A.; Taglieri, G.; Rossi, L.; Gallucci, K. Separation of carbon dioxide for biogas upgrading to biomethane. *J. Clean. Prod.* **2017**, *164*, 1205–1218. [[CrossRef](#)]
22. Choi, S.; Drese, J.H.; Jones, C.W. Adsorbent Materials for Carbon Dioxide Capture from Large Anthropogenic Point Sources. *ChemSusChem* **2009**, *2*, 796–854. [[CrossRef](#)]
23. Drage, T.C.; Snape, C.E.; Stevens, L.A. Materials challenges for the development of solid sorbents for post-combustion carbon capture. *J. Mater. Chem. Interdiscip. J. Deal. Synth. Struct. Prop. Appl. Mater. Part. Those Assoc. Adv. Technol.* **2012**, *22*, 2815–2823. [[CrossRef](#)]
24. Zhao, M.; Xiao, J.; Gao, W.; Wang, Q. Defect-rich Mg-Al MMOs supported TEPA with enhanced charge transfer for highly efficient and stable direct air capture. *J. Energy Chem.* **2022**, *68*, 401–410. [[CrossRef](#)]
25. Muchan, P.; Narku-Tetteh, J.; Saiwan, C.; Idem, R.; Supap, T. Effect of number of amine groups in aqueous polyamine solution on carbon dioxide (CO_2) capture activities. *Sep. Purif. Technol.* **2017**, *184*, 128–134. [[CrossRef](#)]
26. Yang, H.; Wang, X.; Liu, J.; Liu, W.; Gong, Y.; Sun, Y. Amine-impregnated polymeric resin with high CO_2 adsorption capacity for biogas upgrading. *Chem. Eng. J.* **2022**, *430*, 132899. [[CrossRef](#)]
27. Khoshhal Salestan, S.; Pirzadeh, K.; Rahimpour, A.; Abedini, R. Poly (ether-block amide) thin-film membranes containing functionalized MIL-101 MOFs for efficient separation of CO_2/CH_4 . *J. Environ. Chem. Eng.* **2021**, *9*, 105820. [[CrossRef](#)]
28. Zhou, G.; Yang, S.; Tian, Y.; Liu, Y.; Liu, Z.; Dong, X. Adsorption application of tetraethylenetetramine (TEPA) modified SBA-15@MIL-101(Cr) in carbon capture and storage (CCS). *Microporous Mesoporous Mater.* **2022**, *344*, 112232. [[CrossRef](#)]
29. Zhang, G.; Zhao, P.; Hao, L.; Xu, Y. Amine-modified SBA-15(P): A promising adsorbent for CO_2 capture. *J. CO₂ Util.* **2018**, *24*, 22–33. [[CrossRef](#)]
30. Zhao, Y.; Zhu, Y.; Zhu, T.; Lin, G.; Shao, M.; Hong, W.; Hou, S. Polyethylenimine-Based Solid Sorbents for CO_2 Adsorption: Performance and Secondary Porosity. *Ind. Eng. Chem. Res.* **2019**, *58*, 15506–15515. [[CrossRef](#)]
31. Ren, H.; Shen, H.; Liu, Y. Adsorption of CO_2 with tetraethylammonium glycine ionic liquid modified alumina in the Rotating Adsorption Bed. *J. CO₂ Util.* **2022**, *58*, 101925. [[CrossRef](#)]
32. Liu, Y.; Yu, X. Carbon dioxide adsorption properties and adsorption/desorption kinetics of amine-functionalized KIT-6. *Appl. Energy* **2018**, *211*, 1080–1088. [[CrossRef](#)]
33. Serna-Guerrero, R.; Sayari, A. Modeling adsorption of CO_2 on amine-functionalized mesoporous silica. 2: Kinetics and breakthrough curves. *Chem. Eng. J.* **2010**, *161*, 182–190. [[CrossRef](#)]
34. Chaikittisilp, W.; Kim, H.-J.; Jones, C.W. Mesoporous Alumina-Supported Amines as Potential Steam-Stable Adsorbents for Capturing CO_2 from Simulated Flue Gas and Ambient Air. *Energy Fuels* **2011**, *25*, 5528–5537. [[CrossRef](#)]
35. Priyadarshini, P.; Rim, G.; Rosu, C.; Song, M.; Jones, C.W. Direct Air Capture of CO_2 Using Amine/Alumina Sorbents at Cold Temperature. *ACS Environ. Au* **2023**, *3*, 295–307. [[CrossRef](#)] [[PubMed](#)]
36. Chaikittisilp, W.; Khunsupat, R.; Chen, T.T.; Jones, C.W. Poly(allylamine)-Mesoporous Silica Composite Materials for CO_2 Capture from Simulated Flue Gas or Ambient Air. *Ind. Eng. Chem. Res.* **2011**, *50*, 14203–14210. [[CrossRef](#)]
37. Kumar, R.; Ohtani, S.; Tsunogi, N. Direct air capture on amine-impregnated FAU zeolites: Exploring for high adsorption capacity and low-temperature regeneration. *Microporous Mesoporous Mater.* **2023**, *360*, 112714. [[CrossRef](#)]
38. Thakkar, H.; Issa, A.; Rownaghi, A.A.; Rezaei, F. CO_2 Capture from Air Using Amine-Functionalized Kaolin-Based Zeolites. *Chem. Eng. Technol. Ind. Chem. Plant Equip. Process Eng. Biotechnol.* **2017**, *40*, 1999–2007. [[CrossRef](#)]
39. Sun, Y.; Liu, W.; Wang, X.; Yang, H.; Liu, J. Enhanced Adsorption of Carbon Dioxide from Simulated Biogas on PEI/MEA-Functionalized Silica. *Int. J. Environ. Res. Public Health* **2020**, *17*, 1452. [[CrossRef](#)]